applied sciences

MDPI

Article

Event-Triggered Disturbance Estimation and Output Feedback Control Design for Inner-Formation Systems

Liwei Hao [1,*] and Yingchun Zhang [1,2]

[1] Research Center of Satellite Technology, Harbin Institute of Technology, Harbin 150001, China; zhang@hit.edu.cn
[2] Intelligent Control and Aerospace Laboratory, C-Space Intelligent Technology, Hangzhou 310000, China
* Correspondence: haolw@hit.edu.cn

Abstract: This study investigates an event-triggered disturbance estimation approach for the inner-formation system. An extended state observer is designed using an event-based sampling scheme, which offers advantages over traditional estimation methods by reducing information transmission and unnecessary output information exchange while ensuring accurate system estimation performance. Additionally, a method for designing output-feedback control is proposed. The separation of feedback control and event-based observation in the design of output feedback allows us to apply existing optimal control algorithms to the targeted plant without compromising our established event-triggered sampling methods. A numerical simulation is presented, and we demonstrate the effectiveness of our proposed approach for the inner-formation system.

Keywords: inner formation system; drag free control; event-triggered estimation; extended state observer; output feedback

check for updates

Citation: Hao, L.; Zhang, Y. Event-Triggered Disturbance Estimation and Output Feedback Control Design for Inner-Formation Systems. *Appl. Sci.* **2024**, *14*, 3656. https://doi.org/10.3390/app14093656

Academic Editor: Dongsheng Wen

Received: 22 February 2024
Revised: 16 April 2024
Accepted: 20 April 2024
Published: 25 April 2024

Copyright: © 2024 by the authors. Licensee MDPI, Basel, Switzerland. This article is an open access article distributed under the terms and conditions of the Creative Commons Attribution (CC BY) license (https://creativecommons.org/licenses/by/4.0/).

1. Introduction

The inner-formation technology, also known as drag-free control technology [1,2], enables the achievement of pure gravitational orbits crucial in space physics and other domains by effectively compensating for non-conservative forces acting on spacecraft, making it extensively utilized in space science experimental platforms [3–13]. This control method utilizes external actuation to counteract relative motion deviations between the external and internal spacecraft, thereby achieving compensation for interference from the external spacecraft. Due to its significant developmental potential, scholars have conducted extensive research on the inner-formation system [14–18] and drag-free spacecraft [19–32].

In the inner-formation control system, the research focus lies in investigating the dynamics of relative motion between internal and external spacecraft, followed by designing control strategies. However, when studying relative motion characteristics, it is often challenging to directly measure the velocity and acceleration of relative motion as well as external interference sources and uncertainties due to limited sensor capabilities. To address this issue, a modified Unscented Kalman Filter algorithm is employed for estimating the relative motion between the inner satellite and outer satellite in [14]. Additionally, [33] proposes an estimation method for the relative motion state and disturbance of test masses in drag-free satellites based on the self-recurrent wavelet neural network. Moreover, observers can be utilized to analyze the dynamic characteristics of the system. An extended state observer not only estimates the system state but also quantifies additional interference sources and uncertainties. The extended state observer was initially introduced in reference [34], and subsequently developed further with a design approach that incorporates high gain parameters for system gain configuration. Reference [35] provides a comprehensive explanation on designing high-gain extended state observers, which have gained significant attention due to their superior observation efficiency. For a two-test-mass inner-formation drag-free system, an observer-based Model Predictive Control (MPC) is proposed, demonstrating

its feasibility for deep space exploration according to simulation results [36]. Furthermore, active disturbance rejection control incorporating an extended state observer is investigated for achieving frequency domain performance requirements in gravitational detection missions [37].

However, these estimation algorithms encounter a limitation in that they fail to consider the constraints imposed by system information transmission resources when utilizing system output information for state estimation. The system acquires such information through continuous or periodic sampling methods. By adopting event-driven estimation, this issue can be addressed and improved upon. Event-triggered method determines the sampling time of the system by establishing specific triggering conditions, thereby enabling high-frequency sampling during periods requiring more frequent measurements and low-frequency sampling during more stable stages, thus optimizing resource allocation for sampling [38]. Since its inception, event-based estimation has made significant advancements and found applications across diverse domains. In [39], the event-triggered method is considered for a state feedback controller with an input-to-state stability (ISS) result, and the minimum sampling interval is obtained by a Comparison Lemma [40]. The event-triggered method is introduced to spacecraft systems and underwater systems in [41] and [42], respectively; the event-based controller shows its advantage with non-periodic sampling. Additionally, the event-triggered approach is also introduced into estimation design, i.e., event-triggered observers for delay affine systems in [43], event-triggered cascade high-gain observers in [44], and event-triggered observers for one-side Lipschitz systems in [45].

Motivated by this approach, this article proposes an event-driven estimation and output feedback control method for the relative motion equation of internal formation formations. The advantages of the proposed algorithm are as follows: (1) Compared to traditional estimation methods, the process of event-triggered estimation can be more efficiently sampled to minimize the acquisition of unnecessary sampling information by implementing a well-designed triggering mechanism, which initiates sampling only when deemed necessary. (2) In the methodologies proposed in this paper, feedback control and event-triggered observation can be separated. It means that we can leverage existing feedback control algorithms by introducing our event-based extended state observers extensively. The design presented herein is partially similar to the separation principle in continuous design, which is also observed in other works in the literature on observer design, such as in [46]. The event-triggered control method proposed in this paper can theoretically replicate the convergent upper bound achievable through continuous sampling, thereby facilitating more effective utilization of system output information without compromising system performance. This holds significant research implications, as it offers potential improvements and enhancements to existing continuous output feedback control rates based on interference observation under this novel sampling mechanism.

The organizational structure of this article is as follows. Section 2 introduces the plant under consideration and formulates the problem that needs to be addressed. Building upon this, Section 3 presents the main results concerning event-triggered observer for inner-formation dynamics, followed by a proposal for an output feedback control based on the observer. In Section 4, a numerical example is provided to demonstrate the application of our method to a flying plant through numerical simulation. Finally, Section 5 concludes with key findings and outlines future research directions. Additionally, the proofs of the relevant theorems in this paper are provided in the Appendix A.

2. Problem Formulation

In this section, the dynamics we intend to investigate will be presented, while the primary issue that requires resolution is articulated herein. Firstly, let us consider the following relative motion dynamics of inner formation systems:

$$\ddot{r}_{12} + 2n \times \dot{r}_{12} + n \times (n \times r_{12}) + \dot{n} \times r = \frac{f_2}{m_2} - \frac{f_1}{m_1} + u \tag{1}$$

where SC1 and SC2 denote the outer spacecraft and inner spacecraft, respectively, with $r_{12} = \begin{bmatrix} r_1 & r_2 & r_3 \end{bmatrix}$ representing the vector from SC1 to SC2, $n = \begin{bmatrix} n_1 & n_2 & n_3 \end{bmatrix}$ representing the angular velocity of SC1, f_1 and f_2 representing external disturbances acting on SC1 and SC2, respectively, m_1 and m_2 corresponding to the masses of SC1 and SC2, respectively, and u representing the control input for the outer spacecraft. It can be observed that $\ddot{r}_{12}(t)$ comprises both external disturbances and uncertainties, which are collectively represented as $h_i(t)$:

$$\begin{cases} h_1(t) = \Delta a_1 + 2n_3\dot{r}_2 - 2n_2\dot{r}_3 + {n_3}^2 r_1 + {n_2}^2 r_1 - n_2 n_1 r_2 + \dot{n}_3 r_2 - n_3 n_1 r_3 - \dot{n}_2 r_3 \\ h_2(t) = \Delta a_2 - 2n_3\dot{r}_1 + 2n_1\dot{r}_3 - n_2 n_1 r_1 - \dot{n}_3 r_1 + {n_3}^2 r_2 + {n_1}^2 r_2 - n_3 n_2 r_3 + \dot{n}_1 r_3 \\ h_3(t) = \Delta a_3 + 2n_2\dot{r}_1 - 2n_1\dot{r}_2 - n_3 n_1 r_1 + \dot{n}_2 r_1 - n_3 n_2 r_2 - \dot{n}_1 r_2 + {n_2}^2 r_3 + {n_1}^2 r_3 \end{cases} \tag{2}$$

where $\Delta a = \begin{bmatrix} \Delta a_1 & \Delta a_2 & \Delta a_3 \end{bmatrix}^T$ represents the term $\frac{f_2}{m_2} - \frac{f_1}{m_1}$, which means the disturbance and uncertainty of the system. Then, the following assumption is proposed.

Assumption 1. *$h_i(t)$ $(i = 1, 2, 3)$ is derivable, and its derivative is bounded by some positive constant M_i, which means that $\frac{d|h_i(t)|}{dt} \leq M_i$.*

This assumption serves as a fundamental premise in the design of extended observers, enabling us to conduct differential calculations and estimations of the extended state. Building upon this assumption, we elaborate on the key issues that necessitate attention in this article:

1. To propose an event-triggered extended observer for system (1), based on the output information obtained through event-based sampling, providing estimation for all states as well as external disturbances and uncertainties;
2. To design an output feedback controller using the proposed event-triggered observer, ensuring practical applicability in the presence of bounded disturbances and uncertainties;
3. To determine a minimum interval to ensure the absence of Zeno behavior under the proposed sampling scheme.

3. Main Results

This section states the main results in this work, the event-based estimation design is given, and a output feedback is proposed based on the observer.

3.1. Event-Triggered Disturbance Estimation for Relative Motion Dynamics

Considering the dynamics (1), $\varsigma_1(t)$, $\varsigma_2(t)$ $\varsigma_3(t)$ represent the estimation to r_1, r_2 and r_3 respectively, $\psi_1(t)$, $\psi_2(t)$ $\psi_3(t)$ represent the estimation to $\dot{r}_1$, $\dot{r}_2$ and $\dot{r}_3$ respectively, and $\phi_1(t)$, $\phi_2(t)$ $\phi_3(t)$ represent the estimation to $\ddot{r}_1$, $\ddot{r}_2$ and $\ddot{r}_3$, respectively. Since the event-triggered extended observer is proposed as:

$$\begin{aligned} \dot{\xi}_i(t) &= \psi_i(t) + \ell_i \beta_{i1}(r_i(t_k) - \xi_i(t)) \\ \dot{\psi}_i(t) &= \phi_i(t) + \ell_i^2 \beta_{i2}(r_i(t_k) - \xi_i(t)) + u_i(t) \\ \dot{\phi}_i(t) &= \ell_i^3 \beta_{i3}(r_i(t_k) - \xi_i(t)), i = 1, 2, 3 \end{aligned} \tag{3}$$

for any $t \in [t_k, t_{k+1})$, where $u_i(t)$ represent the control input for each axis, $K_i(\beta) = \begin{bmatrix} \beta_{i1} & \beta_{i2} & \beta_{i3} \end{bmatrix}^T$ represents the gain of the observer, ℓ_i is the high-gain parameter, t_k $(k \in \mathbb{N})$ denotes the sampling moment, and the first sampling happens at the initial time t_0. The event-triggered mechanism selectively transmits output information by monitoring at the sensor end, allowing for the separate monitoring and transmission of three-axis output information. The transmission mechanism is designed to trigger sampling based on some positive constants Π_1, Π_2, and Π_3 by design:

$$|r_1(t) - r_1(t_k)| \leq \Pi_1 \tag{4}$$

$$|r_2(t) - r_2(t_k)| \leq \Pi_2 \tag{5}$$

$$|r_3(t) - r_3(t_k)| \leq \Pi_3 \tag{6}$$

The estimation errors are defined as $\tilde{\xi}(t) = r_i(t) - \xi(t)$, $\tilde{\psi}(t) = \dot{r}_i(t) - \psi(t)$ and $\tilde{\phi}(t) = \ddot{r}_i(t) - \phi(t)$. Then, the following theorem is obtained.

Theorem 1. *Let us consider plant (1), observer (14) and the driven conditions (4)–(6) if there exist some positive definite matrices P_1, P_2, P_3, and some constants $\theta > 0$, $0 < \sigma < 1$ such that*

$$0 < \|P_i K_i(\beta)\| \Pi_i \leq \frac{1}{\ell_i{}^3}\left(\frac{\lambda\sigma}{2}\sqrt{\frac{\underline{\varpi}}{\bar{\varpi}}}\theta - \|P_i\| M_i\right), i = 1,2,3 \tag{7}$$

where $\bar{\varpi}$ and $\underline{\varpi}$ represent the maximum and minimum eigenvalues among P_1, P_2, and P_3, respectively. And then, there exists some β_{i1}, β_{i2} and β_{i3} such that the estimation error will meet the bound

$$\left|\tilde{\xi}_i(t)\right| \leq \frac{\theta}{\ell_i^3} \tag{8}$$

$$|\tilde{\psi}_i(t)| \leq \frac{\theta}{\ell_i^2} \tag{9}$$

$$|\tilde{\phi}_i(t)| \leq \frac{\theta}{\ell_i} \tag{10}$$

for any $t \geq t_0 + T(\ell)$, where $\ell = \min\{\ell_1, \ell_2, \ell_3\}$, and $T(\ell)$ is some positive constant which satisfies $\limsup_{\ell\to\infty} T(\ell) = 0$.

Remark 1. *It is a common conclusion to obtain practical convergence in estimates under bounded disturbances. From the fact (A10), we show that the ultimate bound of $\varsigma(t)$*

$$\limsup_{t\to\infty}\left|\tilde{\xi}_i(t)\right| \leq \frac{\theta}{\ell^3}, 1 \leq i \leq 3 \tag{11}$$

$$\limsup_{t\to\infty}|\tilde{\psi}_i(t)| \leq \frac{\theta}{\ell^2}, 1 \leq i \leq 3 \tag{12}$$

$$\limsup_{t\to\infty}|\tilde{\phi}_i(t)| \leq \frac{\theta}{\ell}, 1 \leq i \leq 3 \tag{13}$$

with some constant θ, and it is obvious to obtain same results by continuous extended observer:

$$\begin{aligned} \dot{\xi}_i(t) &= \psi_i(t) + \ell_i\beta_{i1}(r_i(t) - \xi_i(t)) \\ \dot{\psi}_i(t) &= \phi_i(t) + \ell_i^2\beta_{i2}(r_i(t) - \xi_i(t)) + u_i(t) \\ \dot{\phi}_i(t) &= \ell_i^3\beta_{i3}(r_i(t) - \xi_i(t)), i = 1,2,3 \end{aligned} \tag{14}$$

Remark 2. *From the fact (A10), we obtain the ultimate bound $\limsup_{\ell\to\infty}\|\tilde{\xi}_i(t)\| = \limsup_{\ell\to\infty}\|\tilde{\psi}_i(t)\| = \limsup_{\ell\to\infty}\|\tilde{\phi}_i(t)\| = 0$ for any $t \geq t_0$, and this obtained result is in line with the design outcomes of the extended state observer for continuous time sampling. We can indicate that the system convergence upper bound can be enhanced by adjusting parameter ℓ. This advantage remains unchanged even with the introduction of event-triggered mechanisms.*

3.2. Observer-Based Output Feedback Control with Event-Triggered Sampling

Considering the plant (1), our objective is to design an observer-based output-feedback control law using event-based sampling in this subsection. Our analysis approach aims to identify a broad range of output feedback control rates that satisfy the conditions and achieve practical convergence of the system under existing event-triggered estimation,

while incorporating control design and event-driven separation. An output feedback control signal is provided by:

$$\hat{u}_i(t) = \gamma_i(\varsigma_i) \tag{15}$$

The function γ_i presented here is a universally applicable output feedback expression that relies on the system state. Our original design intention was to leverage these states. As long as the control rate of Proposition 1 is satisfied, it can be seamlessly integrated with our event-driven approach to achieve control convergence. Further elucidation regarding the properties of γ_i will be provided in subsequent context. Based on the active disturbance rejection control approach, the controller we use, in fact, is:

$$u_i(t) = \hat{u}_i(t) - \phi_i(t) \tag{16}$$

The following dynamics is given:

$$\begin{bmatrix} \dot{r}_i(t) \\ \ddot{r}_i(t) \\ \dot{\xi}_i(t) \\ \dot{\psi}_i(t) \\ \dot{\phi}_i(t) \end{bmatrix} = \begin{bmatrix} 0 & 1 & 0 & 0 & 0 \\ 0 & 0 & 0 & 0 & 0 \\ \ell_i\beta_{i1} & 0 & -\ell_i\beta_{i1} & 1 & 0 \\ {\ell_i}^2\beta_{i2} & 0 & -{\ell_i}^2\beta_{i2} & 0 & 1 \\ {\ell_i}^3\beta_{i3} & 0 & -{\ell_i}^3\beta_{i3} & 0 & 0 \end{bmatrix} \begin{bmatrix} r_i(t) \\ \dot{r}_i(t) \\ \xi_i(t) \\ \psi_i(t) \\ \phi_i(t) \end{bmatrix} + \begin{bmatrix} 0 & 0 & 0 \\ 1 & 0 & 1 \\ 0 & \ell_i\beta_{i1} & 0 \\ 0 & {\ell_i}^2\beta_{i2} & 1 \\ 0 & {\ell_i}^3\beta_{i3} & 0 \end{bmatrix} \begin{bmatrix} h_i(t) - \phi_i(t) \\ r_i(t_k) - r_i(t) \\ \hat{u}_i(t) \end{bmatrix} \tag{17}$$

Here, we make the following transformation:

$$\begin{bmatrix} \frac{\dot{r}_i(t)}{\ell_i} \\ \frac{\ddot{r}_i(t)}{{\ell_i}^2} \\ \frac{\dot{\xi}_i(t)}{\ell_i} \\ \frac{\dot{\psi}_i(t)}{{\ell_i}^2} \\ \frac{\dot{\phi}_i(t)}{{\ell_i}^3} \end{bmatrix} = \begin{bmatrix} 0 & \ell_i & 0 & 0 & 0 \\ 0 & 0 & 0 & 0 & 0 \\ \ell_i\beta_{i1} & 0 & -\ell_i\beta_{i1} & \ell_i & 0 \\ \ell_i\beta_{i2} & 0 & -\ell_i\beta_{i2} & 0 & \ell_i \\ \ell_i\beta_{i3} & 0 & -\ell_i\beta_{i3} & 0 & 0 \end{bmatrix} \begin{bmatrix} \frac{r_i(t)}{\ell_i} \\ \frac{\dot{r}_i(t)}{{\ell_i}^2} \\ \frac{\xi_i(t)}{\ell_i} \\ \frac{\psi_i(t)}{{\ell_i}^2} \\ \frac{\phi_i(t)}{{\ell_i}^3} \end{bmatrix} + \begin{bmatrix} 0 & 0 & 0 \\ \frac{1}{{\ell_i}^2} & 0 & \frac{1}{{\ell_i}^2} \\ 0 & \beta_{i1} & 0 \\ 0 & \beta_{i2} & \frac{1}{{\ell_i}^2} \\ 0 & \beta_{i3} & 0 \end{bmatrix} \begin{bmatrix} h_i(t) - \phi_i(t) \\ r_i(t_k) - r_i(t) \\ \hat{u}_i(t) \end{bmatrix} \tag{18}$$

For the sake of convenience, we define a new state $\Theta_i = \begin{bmatrix} \frac{r_i}{\ell_i} & \frac{\dot{r}_i}{{\ell_i}^2} & \frac{\xi_i}{\ell_i} & \frac{\psi_i}{{\ell_i}^2} & \frac{\phi_i}{{\ell_i}^3} \end{bmatrix}^T$ and a new function $F(\Theta_i)$:

$$F(\Theta_i) = \begin{bmatrix} 0 & 1 & 0 & 0 & 0 \\ 0 & 0 & 0 & 0 & 0 \\ \beta_{i1} & 0 & -\beta_{i1} & 1 & 0 \\ \beta_{i2} & 0 & -\beta_{i2} & 0 & 1 \\ \beta_{i3} & 0 & -\beta_{i3} & 0 & 0 \end{bmatrix} \Theta_i(t) + \begin{bmatrix} 0 \\ \frac{1}{{\ell_i}^3} \\ 0 \\ \frac{1}{{\ell_i}^3} \\ 0 \end{bmatrix} \hat{u}_i(t) \tag{19}$$

The introduced controller (15) satisfies the following proposition.

Proposition 1. *There exists a Lyapunov function $W(\Theta_i)$ which satisfies the following conditions:*

$$a_1\|\Theta_i\|^2 \le W(\Theta_i) \le a_2\|\Theta_i\|^2 \tag{20}$$

$$\frac{\partial W}{\partial \Theta_i} F(\Theta_i) \le -a_3\|\Theta_i\|^2 \tag{21}$$

$$\left\| \frac{\partial W}{\partial \Theta_i} \right\| \le a_4\|\Theta_i\| \tag{22}$$

where a_1, a_2, a_3, and a_4 are some positive constants.

It is evident that the output feedback control algorithm (15), which satisfies Proposition (1), can achieve exponential convergence of the system without considering estimation errors associated with interference and event-driven introduction. Although the specific

form of the output feedback algorithm employed here remains undefined, various optimization control methods can ultimately be applied. The analysis approach adopted in this study draws inspiration from the continuous-time high-gain observer analysis approach on the separation principle [46]. With bounded interference introduced, the observer does not impose any additional changes to the calculation of control feedback gain for the system. Furthermore, incorporating an event-triggered mechanism does not introduce any extra design burden to the system.

Theorem 2. *Let us consider that plant (1) observer-based output feedback control law (16), states $r(t)$, and $\dot{r}(t)$ will be practically convergent; this means that the states of (1) meet a certain limit bound by the controller (16).*

Theorem 2 proposes the performance of the output-feedback control law, and the proof is presented in the appendix.

Remark 3. *The determination of a convergence interval is an inherent outcome in the design of output feedback control under bounded disturbances, and this outcome remains valid even with the incorporation of event-triggered estimation design.*

Remark 4. *It is obvious that* $\limsup_{\ell_i \to \infty} \left\| e^{-\frac{a_3 \ell_i}{2}(t-t_0)} \right\| = \limsup_{\ell_i \to \infty} \left\| e^{-\frac{\lambda(1-\sigma)\ell_i}{2\delta}(t-t_0)} \right\| = 0$ *holds on, since that we get* $\limsup_{\ell_i \to \infty} \|W_i(t)\| = 0$ *from (A19). It means that we obtain a ultimate boundedness:*

$$\limsup_{\ell_i \to \infty} \|\Theta_i(t)\| = 0 \tag{23}$$

Remark 5. *Here, we propose a general condition for designing output feedback control based on the aforementioned event-triggered extended observer that can be applied to the system. Specifically, after extracting disturbances and event-driven effects, the estimated state information is utilized to design output feedback control, satisfying conditions (20)–(22), thereby ensuring the practicality and convergence of the system. The employed output feedback control method can be a commonly used design approach, and in subsequent design examples, we will also present a simplified design criterion.*

Remark 6. *Decoupling the system is a commonly employed technique in spacecraft control system design. In this study, we propose an observer-based approach to address this issue, which effectively mitigates decoupling-induced errors by estimating and compensating for them using the extended state. The design parameters of each axis can be adjusted based on the specific control requirements of that axis. This article presents a general conclusion that convergence can be achieved by satisfying these requirements.*

3.3. Zeno Behavior Analysis

In the preceding content, we presented evidence of convergence in the observation and control within the system design. Subsequently, we will conduct an analysis on Zeno behavior. The primary objective of event-driven sampling is to ensure a specific time interval between consecutive samples, thereby preventing the occurrence of Zeno behavior. Subsequently, we will delve into an analysis of this crucial aspect. Consequently, the ensuing theorem is presented. The proof of this theorem is presented in the appendix.

Theorem 3. *Let us consider the event-based estimation (14) for system (1); there will exist a minimum interval between every two samples with driven conditions (4)–(6).*

Remark 7. *Theorem 3 establishes the existence of a minimum sampling interval within our proposed driving condition, ensuring that sampling events do not occur continuously. This absence of Zeno behavior is a fundamental prerequisite for event-triggered design, and the event-based design is only*

meaningful under this premise. The introduction of this requirement did not impose any additional parameter constraints, as they were already ensured by the previous design.

4. Numerical Examples

In this section, we present the practical implementation of the algorithm based on the aforementioned design, demonstrated through a specific numerical simulation example. A inner-formation background with specific parameters is given, and its dynamics is with the form of (1). The simulation parameters are selected as follows: the angular velocity vector of the out-spacecraft, denoted as $n^T = \begin{bmatrix} 2 & 5 & 3 \end{bmatrix} \times 10^{-3}$ rad/s, the mass of the out-spacecraft $m_{out} = 250$ kg, and the mass of the in-spacecraft $m_{in} = 1.5$ kg. Here, m_{out} and m_{in} correspond to m_1 and m_2 in (1), respectively. The external disturbance is considered $\Delta a = \begin{bmatrix} 0.001\sin(2t + \frac{\pi}{4}) & -0.003\sin(t + \frac{\pi}{8}) & 0.002\sin(4t + \frac{\pi}{3}) \end{bmatrix}^T N$. Considering the distinct operational scenarios encountered by each axis in practical spacecraft systems, diverse axis parameters were selected herein, and the disturbances experienced during simulation of each axis also vary. Consequently, these disparities may give rise to variations in the simulation specifics of the three-axis system due to the influence of nonlinear dynamics.

Based on these conditions, we propose a parameter turning in detail here. The parameter of the event-triggered observer is considered to be $\ell_1 = \ell_2 = \ell_3 = 6$, $K_i(\beta) = \begin{bmatrix} 1.2252 & 2.2267 & 0.7633 \end{bmatrix}^T$.

Remark 8. *Here, $K_i(\beta)$ is obtained by condition (A4). The calculation method can be obtained through feature root configuration methods or appropriate LMI (Linear Matrix Inequality) calculation methods. In this paper, we present an LMI-based approach for calculating the method. Specifically, we consider the following LMI conditions: $Q_1^T P + PQ_1 - Q_2^T R^T - RQ_2 < 0$, where $Q_1 = \begin{bmatrix} 0 & 1 & 0 \\ 0 & 0 & 1 \\ 0 & 0 & 0 \end{bmatrix}$, $Q_2 = \begin{bmatrix} 1 & 0 & 0 \end{bmatrix}$, P is a positive definite matrix, and R is a matrix of appropriate order. Calculating P and R through the LMI condition, we obtain $K_i(\beta) = P^{-1}R$.*

And a normal output feedback control is considered here. We use

$$u_1(t) = -\frac{1}{50}\begin{bmatrix} 5.2 & 5 & -2 \end{bmatrix}\begin{bmatrix} \xi_1 & \psi_1 & \phi_1 \end{bmatrix}$$

$$u_2(t) = -\frac{1}{50}\begin{bmatrix} 2.5 & 3.5 & 0 \end{bmatrix}\begin{bmatrix} \xi_1 & \psi_1 & \phi_1 \end{bmatrix}$$

$$u_3(t) = -\frac{1}{50}\begin{bmatrix} 6 & 5 & -2 \end{bmatrix}\begin{bmatrix} \xi_1 & \psi_1 & \phi_1 \end{bmatrix}$$

It is obvious to find that the controllers meet the conditions (20)–(22).

The control results are depicted in Figure 1. As evident from the figure, employing an event-driven sampling design, the system converges to a specific range under the output feedback control rate.

The transmission of sampling information is illustrated in Figure 2. It can be observed that during the initial stages of the system, when additional data are required to support control instructions, sampling occurs at a high frequency. However, once the system achieves stability, there is a significant decrease in the sampling rate, thereby indicating the rationality of this resource allocation design.

The estimation results of the three axes in Figures 3–5 demonstrate convergence patterns consistent with the theoretical findings. By ensuring accurate estimations of displacement and velocity, the system disturbances and uncertainties are also estimated within a certain range.

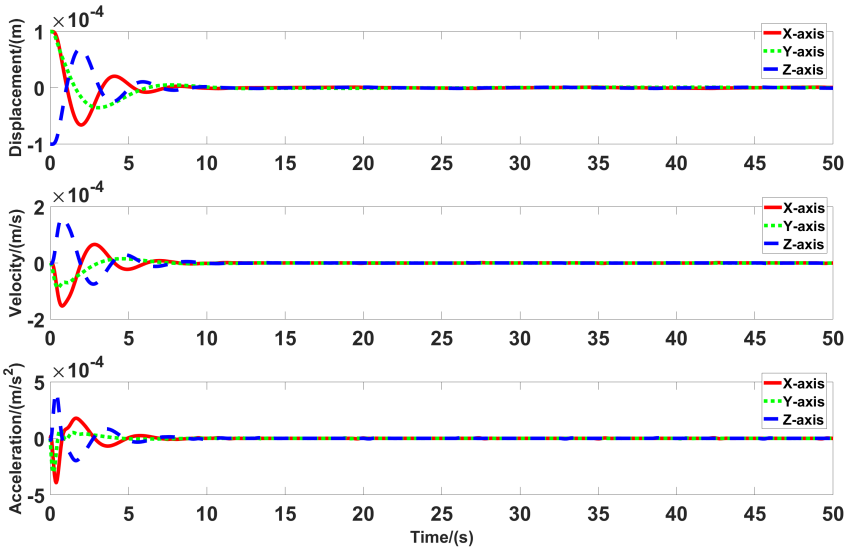

Figure 1. Control results for relative motion.

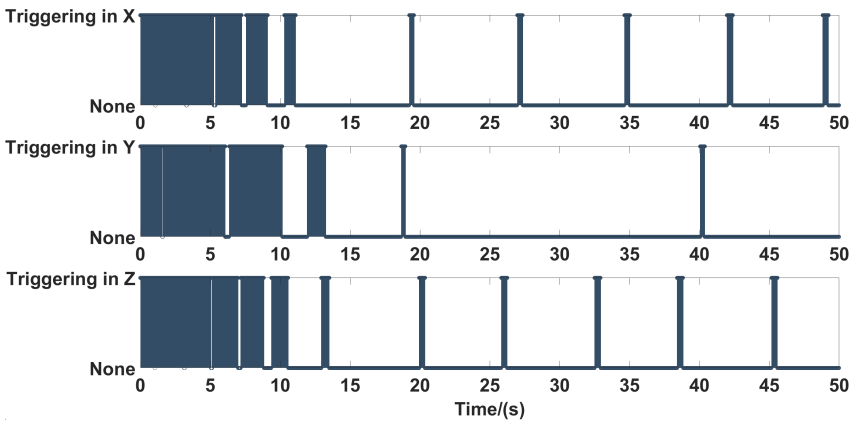

Figure 2. Transmission of sampling information. including the event-driven condition triggering in the X, Y, and Z axes.

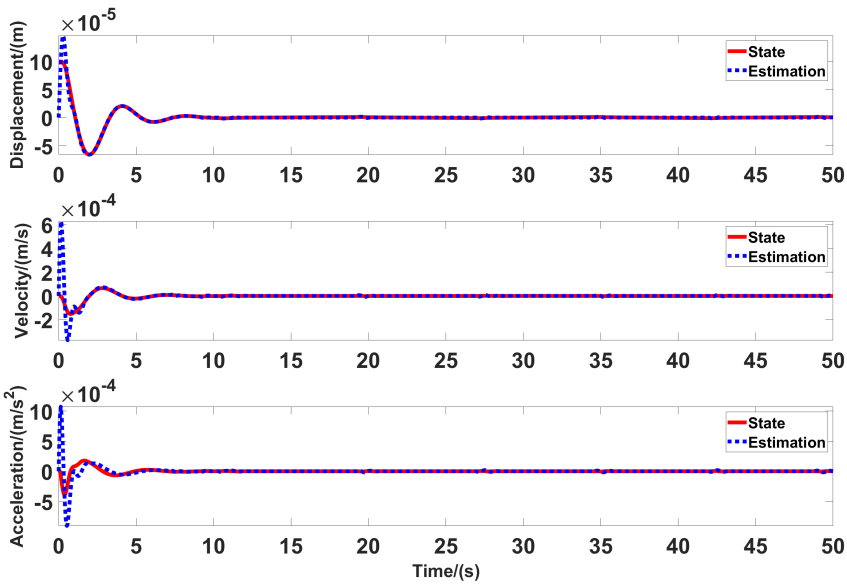

Figure 3. Estimation results for X−axis, including the estimated results of displacement, velocity and acceleration.

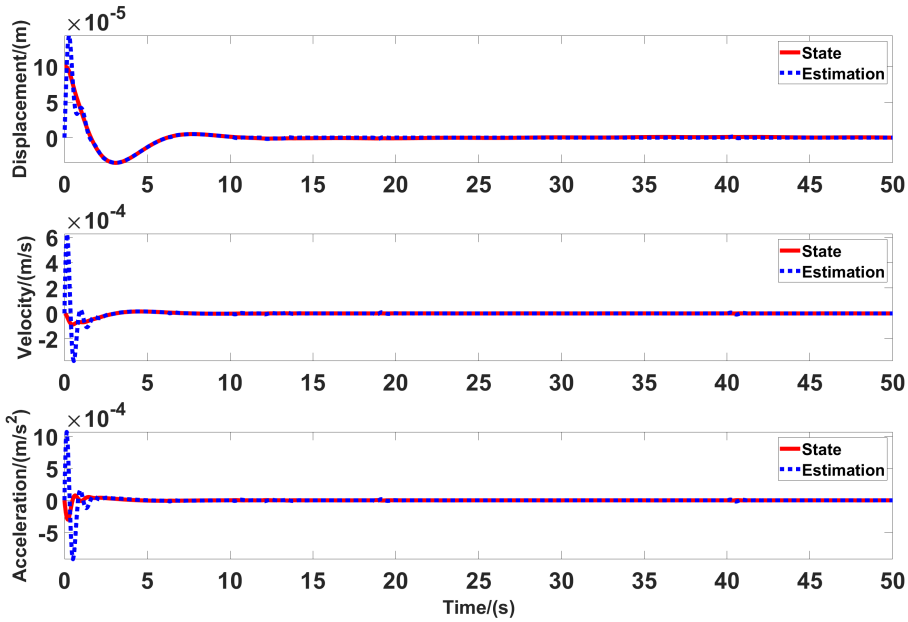

Figure 4. Estimation results for Y−axis, including the estimated results of displacement, velocity and acceleration.

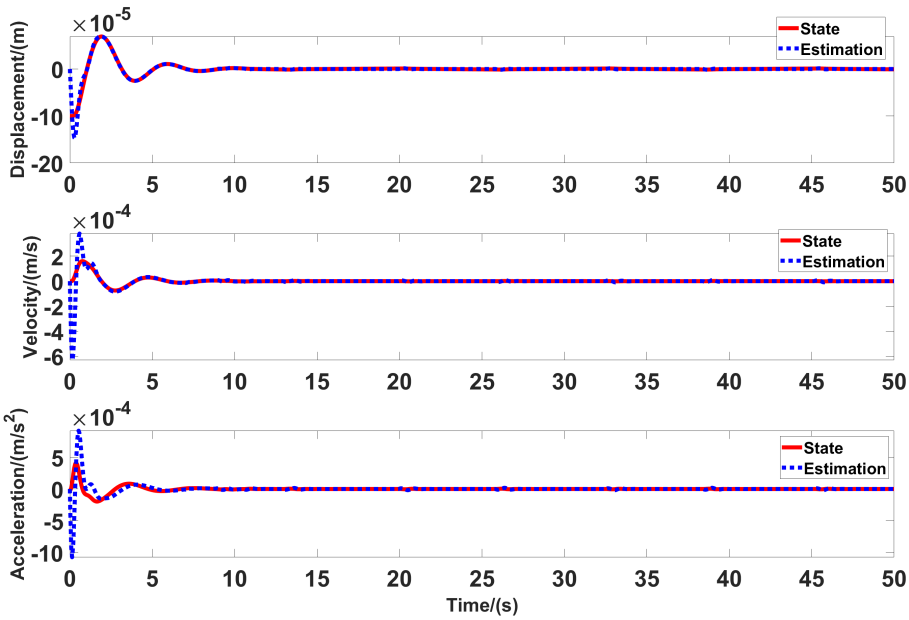

Figure 5. Estimation results for Z−axis, including the estimated results of displacement, velocity and acceleration.

5. Conclusions

The present work addresses an event-based disturbance estimation and output feedback control for inner-formation systems. In this study, we employ an event-triggered extended state observer to estimate the states of the inner-formation system, along with a corresponding output feedback control. By utilizing event-based sampling and avoiding the collection of invalid output information, our designed method achieves bounded estimation errors for the system state in terms of performance. Furthermore, we design output feedback control rates based on the proposed observer, ensuring a separation between the controller and observer that converges to an exact interval under the influence of the control law. We conduct simulations and analyses under specific numerical backgrounds

that conform to relative motion dynamics in an inner formation context, demonstrating the successful application of our design algorithm.

However, it is important to note that certain conservative aspects still exist in these algorithms, such as high sampling frequency during early stages and noise during the sampling process; addressing these issues will be a focus for future solutions. As this study represents a preliminary theoretical investigation into inner-formation systems, our proposed event-triggered control method can theoretically reproduce the convergent upper bound achievable by continuous sampling without affecting system performance, thus offering significant research significance. This implies that existing continuous output feedback control rates based on interference observation can be improved and enhanced under this new sampling mechanism; detailed discussions regarding its application in engineering practice will be presented in future research.

Author Contributions: Conceptualization, L.H. and Y.Z.; data curation, L.H.; formal analysis, L.H.; investigation, L.H.; methodology, L.H.; visualization, L.H.; validation, L.H.; writing—original draft preparation, L.H.; writing—review and editing, L.H. and Y.Z.; supervision, Y.Z.; observations, L.H. and Y.Z. All authors have read and agreed to the published version of the manuscript.

Funding: We are grateful for the support from Guangdong Major Project of Basic and Applied Basic Research (Grant No. 2019B030302001).

Institutional Review Board Statement: Not applicable.

Informed Consent Statement: Not applicable.

Data Availability Statement: The raw data supporting the conclusions of this article will be made available by the authors on request.

Acknowledgments: We are grateful for the support from Tianqin Center, Sun Yat-Sen University, a well as the comments and suggestions from the reviewers and editors.

Conflicts of Interest: The authors declare no conflicts of interest.

Appendix A. Proof of the Theorems

In this appendix, we will present the proofs of all theorems in the main findings of the article, encompassing Theorems 1–3.

Proof of Theorem 1. Firstly, we define the following transformed error $\varsigma(t)$:

$$\varsigma_i(t) = \begin{bmatrix} \ell_i^{-1} & \ell_i^{-2} & \ell_i^{-3} \end{bmatrix} \begin{bmatrix} \tilde{\xi}_i(t) & \tilde{\psi}_i(t) & \tilde{\phi}_i(t) \end{bmatrix}^T, i = 1,2,3 \tag{A1}$$

Combining the dynamics (1) and the event-triggered extended observer (14), we obtain that

$$\begin{aligned} \dot{\varsigma}_i(t) &= \ell_i A \varsigma_i(t) - \ell_i K_i(\beta) \frac{r_i(t_k) - \xi_i(t)}{\ell_i} + \frac{1}{{\ell_i}^3} B \frac{dh_i(t)}{dt} \\ &= \ell_i A \varsigma_i(t) - \ell_i K_i(\beta) C \varsigma_i(t) + K_i(\beta)(r_i(t) - r_i(t_k)) + \frac{1}{{\ell_i}^3} B \frac{dh_i(t)}{dt} \end{aligned} \tag{A2}$$

where $A = \begin{bmatrix} 0 & 1 & 0 \\ 0 & 0 & 1 \\ 0 & 0 & 0 \end{bmatrix}$, $B = \begin{bmatrix} 0 \\ 0 \\ 1 \end{bmatrix}$, $C = \begin{bmatrix} 1 & 0 & 0 \end{bmatrix}$. And then, we consider the Lyapunov function $V(t) = \sum_{i=1}^{3} V_i(t)$, where $V_i(t) = \varsigma_i(t)^T P_i \varsigma_i(t)$. Calculating the derivative of $V_1(t)$, we have:

$$\begin{aligned} \dot{V}_1(t) = \quad & \ell_1 \varsigma_1(t)^T \left(P_1 A + A^T P_1 - P_1 K_1(\beta) C - C^T K_1(\beta)^T P_1 \right) \varsigma_1(t) \\ & + 2\varsigma_1(t)^T P_1 K_1(\beta)(r_1(t) - r_1(t_k)) + \frac{2}{\ell^3} \varsigma_1(t)^T P_1 B \frac{dh_1(x,t)}{dt} \end{aligned} \tag{A3}$$

By choosing β_{11}, β_{12} and β_{13}, it satisfies that the roots of function

$$s^3 + \beta_{11}s^2 + \beta_{12}s + \beta_{13} = 0 \tag{A4}$$

have negative real parts. From (A4), we show that $A - K_i(\beta)C$ is Hurwitz since then there exists a positive constant λ such that

$$\begin{aligned}\dot{V}_1(t) &= -\lambda\ell_1\varsigma_1(t)^T\varsigma_1(t) + 2\varsigma_1(t)^T P_1 K_1(\beta)(r_1(t) - r_1(t_k)) + \frac{2}{\ell_1^3}\varsigma_1{}^T P_1 B\frac{dh_1(t)}{dt} \\ &\le -\lambda\ell_1\|\varsigma_1(t)\|^2 + 2\|\varsigma_1(t)\|\|P_1K_1(\beta)\||r_1(t) - r_1(t_k)| + \frac{2}{\ell_1^3}\|\varsigma_1(t)\|\|P_1\|\left|\frac{dh_1(t)}{dt}\right|\end{aligned} \tag{A5}$$

Combining the Assumption 1 and the driven condition (4), we have that

$$\dot{V}_1 \le -\lambda\ell(1-\sigma)\|\varsigma_1\|^2 - \lambda\sigma\ell\|\varsigma_1\|^2 + 2\|\varsigma_1\|\|PK(\beta)\|\Pi_1 + \frac{2}{\ell^3}\|\varsigma_1\|\|P\|M_1 \tag{A6}$$

holds for any positive constant $\sigma \in (0,1)$, then we know that

$$\dot{V}_1 \le -\lambda\ell(1-\sigma)\|\varsigma_1\|^2, \forall\|\varsigma_1\| \ge \frac{2}{\lambda\sigma\ell}\|PK(\beta)\|\Pi_1 + \frac{2}{\lambda\sigma\ell^4}\|P\|M_1 \tag{A7}$$

And then, we obtain the inequality

$$\|V_1(t)\| \le \max\left\{\|V(t_0)\|e^{-\frac{\lambda(1-\sigma)\ell_1}{\bar{\varpi}}(t-t_0)}, \bar{\varpi}\left(\frac{2}{\lambda\sigma\ell}\|PK(\beta)\|\Pi_1 + \frac{2}{\lambda\sigma\ell^4}\|P\|M_1\right)^2\right\} \tag{A8}$$

by the result of ultimate boundedness in [40]. Here, we denote the maximum and minimum eigenvalues of P as $\bar{\varpi}$ and $\underline{\varpi}$, respectively, and we have $\underline{\varpi}\|\zeta_1(t)\|^2 \le V(t) \le \bar{\varpi}\|\zeta_1(t)\|^2$. And then, we obtain

$$\|\varsigma_1(t)\| \le \sqrt{\frac{\bar{\varpi}}{\underline{\varpi}}}\max\left\{\|\varsigma_1(t_0)\|e^{-\frac{\lambda(1-\sigma)\ell_1}{2\bar{\varpi}}(t-t_0)}, \frac{2}{\lambda\sigma\ell}\|PK(\beta)\|\Pi_1 + \frac{2}{\lambda\sigma\ell^4}\|P\|M_1\right\} \tag{A9}$$

By substituting condition (7), we have

$$\|\varsigma_1(t)\| \le \max\left\{\sqrt{\frac{\bar{\varpi}}{\underline{\varpi}}}\|\varsigma_1(t_0)\|e^{-\frac{\lambda(1-\sigma)\ell_1}{2\bar{\varpi}}(t-t_0)}, \frac{\theta}{\ell^4}\right\} \tag{A10}$$

We show that

$$\|\varsigma_1(t_0)\|e^{-\frac{\lambda\ell_1}{4\bar{\varpi}}(t-t_0)} \le \frac{\theta}{\ell_1^4} \tag{A11}$$

holds for any

$$t \ge t_0 + \frac{4\bar{\varpi}}{\lambda\ell_1}\ln\frac{\ell_1^4\|\varsigma_1(t_0)\|}{\theta} \tag{A12}$$

Due to the fact that $\lim_{\ell_1\to\infty}\frac{4\bar{\varpi}}{\lambda\ell_1}\ln\frac{\ell_1{}^4\|\varsigma_1(t_0)\|}{\theta} = \lim_{\ell_1\to\infty}\frac{4\bar{\varpi}\theta}{\lambda\ell_1{}^4\|\varsigma_1(t_0)\|} = 0$, we obtain that $\|\varsigma_1(t_0)\| \le \frac{\theta}{\ell_1^4}$ holds for any $t \ge t_0 + T(\ell_1)$, where $T(\ell_1) = \frac{4\bar{\varpi}}{\lambda\ell_1}\ln\frac{\ell^4\|\varsigma_1(t_0)\|}{\theta}$. Similarly, the following conclusion is obtained for another two axis: $\|\varsigma_i(t_0)\| \le \frac{\theta}{\ell_i^4}$ holds for any $t \ge t_0 + T(\ell_i)$, where $T(\ell_i) = \frac{4\bar{\varpi}}{\lambda\ell_i}\ln\frac{\ell_i^4\|\varsigma_i(t_0)\|}{\theta}$, here i = 2, 3.

Consequently, we obtain that conclusions (8)–(10) hold for any $t \ge t_0 + T(\ell)$ by the transformed relationship (A1), where $T(\ell) = \max\{T(\ell_1), T(\ell_2), T(\ell_3)\}$. $\lim_{\ell\to\infty} T(\ell) = 0$ holds obviously, and that ends the proof. □

Proof of Theorem 2. Firstly, we rewrite (18) as follows:

$$\dot{\Theta}_i(t) = \ell_i F(\Theta_i) + J_i \begin{bmatrix} h_i(t) - \phi_i(t) \\ r_i(t_k) - r_i(t) \end{bmatrix} \tag{A13}$$

where $J_i = \begin{bmatrix} 0 & \frac{1}{\ell_i^2} & 0 & 0 & 0 \\ 0 & 0 & \beta_{i1} & \beta_{i2} & \beta_{i3} \end{bmatrix}^T$. Based on this, we calculate the derivative of W_i as follows:

$$\frac{dW_i}{dt} = \frac{\partial W_i}{\partial \Theta_i}\left(\ell_i F(\Theta_i) + J_i \begin{bmatrix} h_i(t) - \phi_i(t) \\ r_i(t_k) - r_i(t) \end{bmatrix}\right) \tag{A14}$$

Substituting conditions (20)–(22) into (A14), we have

$$\begin{aligned} \dot{W}_i(t) \leq & \; -a_3\ell_i\|\Theta_i\|^2 + a_4\|\Theta_i\|\left\|J_i \begin{bmatrix} h_i(t) - \phi_i(t) \\ r_i(t_k) - r_i(t) \end{bmatrix}\right\| \\ \leq & \; -\frac{a_3\ell_i}{2}\|\Theta\|^2 + \frac{{a_4}^2}{2a_3\ell_i}\left\|J_i \begin{bmatrix} h_i(t) - \phi_i(t) \\ r_i(t_k) - r_i(t) \end{bmatrix}\right\|^2 \end{aligned} \tag{A15}$$

According to the design of the extended state observer and the event-triggered mechanism, it is obvious that inequalities

$$|r_i(t_k) - r_i(t)| \leq \Pi_i \leq \frac{1}{\|P_iK_i(\beta)\|{\ell_i}^3}\left(\frac{\lambda\sigma}{2}\sqrt{\frac{\underline{\varpi}}{\bar{\varpi}}}\theta - \|P_i\|M_i\right) \tag{A16}$$

and

$$\begin{aligned} \frac{1}{{\ell_i}^3}|h_i(x) - \phi_i| \leq & \; \max\left\{\|\varsigma_i(t_0)\|\sqrt{\frac{\bar{\varpi}}{\underline{\varpi}}}e^{-\frac{\lambda(1-\sigma)\ell_i}{2\bar{\varpi}}(t-t_0)}, \frac{\theta}{\ell_i^3}\right\} \\ \leq & \; \|\varsigma_i(t_0)\|\sqrt{\frac{\bar{\varpi}}{\underline{\varpi}}}e^{-\frac{\lambda(1-\sigma)\ell_i}{2\bar{\varpi}}(t-t_0)} + \frac{\theta}{\ell_i^4} \end{aligned} \tag{A17}$$

hold. Combining (A16) and (A17), we have

$$\begin{aligned} \left\|J_i \begin{bmatrix} h_i(t) - \phi_i(t) \\ r_i(t_k) - r_i(t) \end{bmatrix}\right\|^2 \leq & \left(\frac{|h_i(t) - \phi_i(t)|}{{\ell_i}^4}\right)^2 + \left[\frac{4\beta_0}{\lambda\|P_iK_i(\beta)\|{\ell_i}^3}\left(\frac{\lambda\sigma\theta}{2}\sqrt{\frac{\underline{\varpi}}{\bar{\varpi}}} - \|P_i\|M_i\right)\right]^2 \\ \leq & \; 2\left(\frac{1}{\ell_i}\|\varsigma_i(t_0)\|\sqrt{\frac{\bar{\varpi}}{\underline{\varpi}}}e^{-\frac{\lambda(1-\sigma)\ell_i}{2\bar{\varpi}}(t-t_0)} + \frac{\delta_i\theta}{\ell_i^3}\right)^2 \end{aligned} \tag{A18}$$

where β_0 is some positive constant independent of ℓ_i, and $\delta_i = \max\left\{\frac{1}{{\ell_i}^2}, \frac{2\beta_0\lambda\sigma}{\lambda\|P_iK_i(\beta)\|}\sqrt{\frac{\underline{\varpi}}{\bar{\varpi}}}\right\}$. The influence caused by external disturbance and event-triggered sampling is proved to be bounded in (A18). After that, we solve $W_i(t)$ from (A15), then the following inequality is obtained:

$$W_i(t) \leq e^{-\frac{a_3\ell_i}{2}(t-t_0)}V_i(t_0) + \int_{t_0}^{t} e^{-\frac{a_3\ell_i}{2}(t-s)}\frac{{a_4}^2}{a_3\ell_i}\left(\frac{1}{\ell_i}\|\varsigma_i(t_0)\|\sqrt{\frac{\bar{\varpi}}{\underline{\varpi}}}e^{-\frac{\lambda(1-\sigma)\ell_i}{2\bar{\varpi}}(t-t_0)} + \frac{\delta_i\theta}{\ell_i^3}\right)^2 ds \tag{A19}$$

After that, the following bound is obtained:

$$\limsup_{t\to\infty} W_i(t) \leq \frac{2{a_4}^2}{{a_3}^2\ell_i^2}\left(\frac{\delta_i\theta}{\ell_i^3}\right)^2 \tag{A20}$$

According to condition (20), we obtain

$$\limsup_{t\to\infty}\|\Theta_i(t)\| \leq \frac{\sqrt{2}a_4}{a_1a_3}\frac{\delta_i\theta}{\ell_i^4} \tag{A21}$$

This result concludes the demonstration. □

Proof of Theorem 3. From the result (A21), we show that

$$W_i(t) \leq V_i(t_0) + \frac{{a_4}^2}{a_3}\|J_i\|^2\left(\|\varsigma_i(t_0)\|\sqrt{\frac{\bar{\varpi}}{\underline{\varpi}}} + \frac{\delta_i\theta}{{\ell_i}^4}\right)^2\frac{2}{a_3} \tag{A22}$$

Here, we define $R_i = V_i(t_0) + \frac{{a_4}^2}{a_3}\|J_i\|^2\left(\|\varsigma_i(t_0)\|\sqrt{\frac{\bar{\varpi}}{\underline{\varpi}}} + \frac{\delta_i\theta}{{\ell_i}^4}\right)^2\frac{2}{a_3}$, then we have $|r_i(t)| \leq \frac{\sqrt{R_i}}{a_1}$, $|\dot{r}_i(t)| \leq \frac{\sqrt{R_i}}{a_1}$ for any $t \geq t_0$. After that, we obtain

$$\begin{aligned} \frac{d(r_i(t) - r_i(t_k))^2}{dt} &= 2(r_i(t) - r_i(t_k))\dot{r}_i(t) \leq 2|r_i(t) - r_i(t_k)||\dot{r}_i(t)| \\ &\leq 2(|r_i(t)| + |r_i(t_k)|)|\dot{r}_i(t)| \leq \frac{4R_i}{{a_1}^2} \end{aligned} \tag{A23}$$

The minimum sampling interval corresponds to the time required for the driving mechanism to regenerate from 0 to the threshold specified in the driving conditions after the previous trigger event. Consequently, by establishing an upper bound on the derivative of the driving mechanism, we can derive a lower bound on the necessary time interval based on both the threshold and this upper bound. According to the driven mechanism (4)–(6), we obtain the minimum interval between each of the two sampling behaviors:

$$\Delta t_{\min} = \frac{{a_1}^2{\Pi_i}^2}{4R_i} \tag{A24}$$

Therefore, Zeno behavior will not happen based on (A24). □

References

1. Dang, Z.; Zhang, Y. Control design and analysis of an inner-formation flying system. *IEEE Trans. Aerosp. Electron. Syst.* **2015**, *51*, 1621–1634. [CrossRef]
2. Lange, B. The drag-free satellite. *AIAA J.* **1964**, *2*, 1590–1606. [CrossRef]
3. Van Patten, R.A.; Everitt, C.W.F. Possible Experiment with Two Counter-Orbiting Drag-Free Satellites to Obtain a New Test of Einstein's General Theory of Relativity and Improved Measurements in Geodesy. *Phys. Rev. Lett.* **1976**, *36*, 629–632. [CrossRef]
4. Armano, M.; Audley, H.; Baird, J.; Binetruy, P.; Born, M.; Bortoluzzi, D.; Castelli, E.; Cavalleri, A.; Cesarini, A.; Cruise, A.M.; et al. LISA Pathfinder Performance Confirmed in an Open-Loop Configuration: Results from the Free-Fall Actuation Mode. *Phys. Rev. Lett.* **2019**, *123*, 111101. [CrossRef]
5. Touboul, P.; Métris, G.; Rodrigues, M.; Bergé, J.; Robert, A.; Baghi, Q.; André, Y.; Bedouet, J.; Boulanger, D.; Bremer, S.; et al. *MICROSCOPE* Mission: Final Results of the Test of the Equivalence Principle. *Phys. Rev. Lett.* **2022**, *129*, 121102. [CrossRef]
6. Abich, K.; Abramovici, A.; Amparan, B.; Baatzsch, A.; Okihiro, B.B.; Barr, D.C.; Bize, M.P.; Bogan, C.; Braxmaier, C.; Burke, M.J.; et al. In-Orbit Performance of the GRACE Follow-on Laser Ranging Interferometer. *Phys. Rev. Lett.* **2019**, *123*, 031101. [CrossRef]
7. Drinkwater, M.R.; Floberghagen, R.; Haagmans, R.; Muzi, D.; Popescu, A. GOCE: ESA's First Earth Explorer Core Mission. *Space Sci. Rev.* **2003**, *108*, 419–432. [CrossRef]
8. Kremer, K.; Chatterjee, S.; Breivik, K.; Rodriguez, C.L.; Larson, S.L.; Rasio, F.A. LISA Sources in Milky Way Globular Clusters. *Phys. Rev. Lett.* **2018**, *120*, 191103. [CrossRef]
9. Schumaker, B. Disturbance reduction requirements for LISA. *Class. Quantum Gravity* **2003**, *20*, S239–S253. [CrossRef]
10. Luo, J.; Chen, L.S.; Duan, H.Z.; Gong, Y.G.; Hu, S.; Ji, J.; Liu, Q.; Mei, J.; Milyukov, V.; Sazhin, M.; et al. TianQin: A space-borne gravitational wave detector. *Class. Quantum Gravity* **2016**, *33*, 035010. [CrossRef]
11. Hu, X.C.; Li, X.H.; Wang, Y.; Feng, W.F.; Zhou, M.Y.; Hu, Y.M.; Hu, S.C.; Mei, J.W.; Shao, C.G. Fundamentals of the orbit and response for TianQin. *Class. Quantum Gravity* **2018**, *35*, 095008. [CrossRef]
12. Gerardi, D.; Allen, G.; Conklin, J.W.; Sun, K.X.; DeBra, D.; Buchman, S.; Gath, P.; Fichter, W.; Byer, R.L.; Johann, U. Advanced drag-free concepts for future space-based interferometers: Acceleration noise performance. *Rev. Sci. Instrum.* **2014**, *85*, 1590–1606. [CrossRef]
13. Liu, H.; Luo, Z.; Jin, G. The development of phasemeter for Taiji space gravitational wave detection. *Microgravity Sci. Technol.* **2018**, *30*, 775–781. [CrossRef]
14. Dang, Z.; Zhang, Y. Relative position and attitude estimation for inner-formation gravity measurement satellite system. *Acta Astronaut* **2011**, *69*, 514–525. [CrossRef]
15. Dang, Z.; Zhang, Y. The principle of solar radiation for controlling a spherical proof mass in an inner-formation satellite. *Acta Astronaut* **2011**, *69*, 860–868. [CrossRef]

16. Gu, Z.; Wang, Z.; Zhang, Y. Analysis of residual gas disturbance on the inner satellite of Inner Formation Flying System. *Sci. China Technol. Sci.* **2012**, *55*, 2511–2517. [CrossRef]
17. Gu, Z.; Wang, Z.; Zhang, Y. Compensation of gravitational attraction disturbance to pure gravity orbit for Inner Formation Flying System. *Acta Astronaut* **2012**, *81*, 635–644. [CrossRef]
18. Dang, Z.; Tang, S.; Xiang, J.; Zhang, Y. Rotational and translational integrated control for Inner-formation Gravity Measurement Satellite System. *Acta Astronaut* **2012**, *75*, 136–153. [CrossRef]
19. Canuto, E.S. Drag-free and attitude control for the GOCE satellite. *Automatica* **2008**, *44*, 1766–1780. [CrossRef]
20. Fichter, W.; Schleicher, A.; Bennani, S.; Wu, S. Closed loop performance and limitations of the LISA pathfinder drag-free control system. In Proceedings of the AIAA Guidance, Navigation, and Control Conference and Exhibit, Hilton Head , SC, USA, 20–23 August 2007.
21. Delavault, S.; Prieur, P.; Liénart, T.; Robert, A.; Guidotti, P.Y. MICROSCOPE mission: Drag-free and attitude control system expertise activities toward the scientific team. *CEAS Space J.* **2018**, *10*, 487–500. [CrossRef]
22. Liao, H.; Xu, Y.; Zhu, Z.; Deng, Y.; Zhao, Y. A new design of drag-free and attitude control based on non-contact satellite. *ISA Trans.* **2019**, *88*, 62–72. [CrossRef]
23. Canuto, E.; Massotti, L.; Molano-Jimenez, A.; Perez, C.N. Drag-free and attitude control for long-distance, low-Earth-orbit, gravimetric satellite formation. In Proceedings of the 29th Chinese Control Conference, Beijing, China, 29–31 July 2011.
24. Ji, L.; Liu, K.; Xiang, J. On all-propulsion design of integrated orbit and attitude control for inner-formation gravity field measurement satellite. *Sci. China Technol. Sci.* **2011**, *54*, 3233–3242. [CrossRef]
25. Grynagier, A.; Ziegler, T.; Fichter, W. Identification of dynamic parameters for a one-axis drag-free gradiometer. *IEEE Trans. Aerosp. Electron. Syst.* **2013**, *49*, 341–355. [CrossRef]
26. Xiao, C.; Bai, Y.; Li, H.; Liu, L.; Liu, Y.; Luo, J.; Ma, Y.; Qu, S.; Tan, D.; Wang, C.; et al. Drag-free control design and in-orbit validation of TianQin-1 satellite. *Class. Quantum Gravity* **2022**, *39*, 155001. [CrossRef]
27. Gath, P.; Fichter, W.; Kersten, M.; Schleicher, A. Drag free and attitude control system design for the LISA Pathfinder mission. In Proceedings of the AIAA Guidance, Navigation, and Control Conference and Exhibit, RI , USA, 16–19 August 2004.
28. Wu, S.F.; Fertin, D. Spacecraft drag-free attitude control system design with quantitative feedback theory, *Acta Astronaut* **2008**, *62*, 668–682. [CrossRef]
29. Gath, P.F.; Schulte, H.R. Drag free and attitude control system design for the LISA science mode. In Proceedings of the AIAA Guidance, Navigation, and Control Conference and Exhibit, Hilton Head, SC, USA, 20–23 August 2007.
30. Sun, X.; Shen, Q.; Wu, S. Partial State Feedback MRAC-Based Reconfigurable Fault-Tolerant Control of Drag-Free Satellite with Bounded Estimation Error, *IEEE Trans. Aerosp. Electron. Syst.* **2023**, *59*, 6570–6586.
31. Sun, X.; Shen, Q.; Wu, S. Event-triggered robust model reference adaptive control for drag-free satellite. *Adv. Space Res.* **2023**, *72*, 4984–4996. [CrossRef]
32. Lian, X.; Zhang, J.; Lu, L.; Wang, J.; Liu, L.; Sun, J.; Sun, Y. Frequency Separation Control for Drag-Free Satellite with Frequency-Domain Constraints. *IEEE Trans. Aerosp. Electron. Syst.* **2021**, *57*, 4085–4096. [CrossRef]
33. Lian, X.; Zhang, J.; Wang, J.; Wang, P; Lu, Z. State and disturbance estimation for test masses of drag-free satellites based on self-recurrent wavelet neural network. *Adv. Space Res.* **2021**, *67*, 3654–3666.
34. Zeitz, M. The extended Luenberger observer for nonlinear systems. *Syst. Control Lett.* **1987**, *9*, 149–156. [CrossRef]
35. Khalil, K. Extended High-Gain Observers as Disturbance Estimators. *SICE J. Control. Meas. Syst. Integr.* **2017**, *10*, 125–134. [CrossRef]
36. Hao, L.; Zhang, J.; Wang, J.; Zhang, J. Extended observer and output feedback control for the preliminary design of tianqin two-test-mass drag-free and attitude control system. In Proceedings of the International Astronautical Congress, Virtual, Online, 12–14 October 2020.
37. Zhang, C.; He, J.; Duan, L.; Kang, Q. Design of an Active Disturbance Rejection Control for Drag-Free Satellite. *Microgravity Sci. Technol.* **2019**, *31*, 31–48. [CrossRef]
38. Heemels, W.P.; Johansson, K.H.; Tabuada, P. An introduction to event-triggered and self-triggered control. In Proceedings of the IEEE 51st IEEE Conference on Decision and Control (CDC), Maui, HI, USA, 10–13 December 2012.
39. Tabuada, P. Event-Triggered Real-Time Scheduling of Stabilizing Control Tasks. *IEEE Trans. Autom. Control* **2007**, *52*, 1680–1685. [CrossRef]
40. Khalil, H.K. *Nonlinear Control*; Pearson: Boston, MA, USA, 2015; pp. 87–90. 354.
41. Xie, X.; Sheng, T.; He, L. Distributed Attitude Synchronization for Spacecraft Formation Flying via Event-Triggered Control. *Appl. Sci.* **2020**, *65*, 4824–4831. [CrossRef]
42. Batmani, Y.; Najafi, S. Event-Triggered H-∞ Depth Control of Remotely Operated Underwater Vehicles. *IEEE Trans. Syst. Man Cybern. Syst.* **2021**, *51*, 1224–1232. [CrossRef]
43. Song, C.; Wang, H.; Tian, Y.; Zheng, G. Event-Triggered Observer Design for Delayed Output-Sampled Systems. *IEEE Trans. Autom. Control* **2020**, *65*, 4824–4831. [CrossRef]
44. Liu, W.; Huang, J. Event-triggered cascade high-gain observer and its application. *Int. J. Robust Nonlinear Control* **2020**, *30*, 2335–2351. [CrossRef]

45. Wang, X.; Park, J.H. State-Based Dynamic Event-Triggered Observer for One-Sided Lipschitz Nonlinear Systems with Disturbances. *IEEE Trans. Circuits Syst. II Express Briefs* **2022**, *69*, 2326–2330. [CrossRef]
46. Khalil, K. Cascade high-gain observers in output feedback control. *Automatica* **2017**, *80*, 110–118. [CrossRef]

Disclaimer/Publisher's Note: The statements, opinions and data contained in all publications are solely those of the individual author(s) and contributor(s) and not of MDPI and/or the editor(s). MDPI and/or the editor(s) disclaim responsibility for any injury to people or property resulting from any ideas, methods, instructions or products referred to in the content.